Electrostatic Simulations of Interactions Between a Scanning Probe and Quantum Hall Liquid

by

Nemanja Ljuban Spasojevic

Submitted to the Department of Physics
in partial fulfillment of the requirements for the degree of

Candidate for Bachelor of Physics

at the

MASSACHUSETTS INSTITUTE OF TECHNOLOGY

February 2006

© Massachusetts Institute of Technology 2006. All rights reserved.

Author . . . .
Department of Physics
May 06, 2005

Certified by . . . .
Raymond Ashoori
Professor
Thesis Supervisor

Certified by . . . .
Gary Steele
Graduate Student
Thesis Supervisor

Accepted by . . . .
David E. Pritchard
Thesis Coordinator

Electrostatic Simulations of Interactions Between a Scanning Probe and Quantum Hall Liquid

by

Nemanja Ljuban Spasojevic

Submitted to the Department of Physics
on May 06, 2005, in partial fulfillment of the
requirements for the degree of
Candidate for Bachelor of Physics

Abstract

In this thesis we modelled interactions between metal probe and quantum Hall liquid. The setup geometries were similar to those met in scanning capacitance microscopy experiments carried out by Ashoori's group [1]. The main interest was to explore the 2DEG charge densities for a different system geometries, magnetic field applied, and tip voltages. We modelled quantum bubble formation under the metal probe, incompressible strip formation beneath the edge of the metal gate, and 2DEG density profile under the influence of donors in magnetic field. In order to model complex geometry systems, but also optimize running times and memory allocation we developed two electrostatic simulators one for cylindrically symmetric and second for arbitrary 3D geometries. Our electrostatic solver was based on successive over relaxation algorithm, but it was optimized for better stability and faster convergence times.

Thesis Supervisor: Raymond Ashoori
Title: Professor

Thesis Supervisor: Gary Steele
Title: Graduate Student

Acknowledgments

I would like to thank to Gary Steele and Ray Ashoori for the guidance and support for the last tree years. Through discussions and many diligent tests step by step we build up fully functional, fast, and robust electrostatic simulator. Also I would like to thank to the UROP office which made all this work possible. And finally I would like to thank to may family for constant support.

Chapter 1

Introduction

In this chapter we will give a brief review on scanning capacitance microscopy experiments. In addition we will introduce concept of two dimensional electron gas (2DEG) systems and their architecture. Later we will review Quantum Hall effects that play important role in physics of 2DEG. Finally in this chapter we will introduce scanning capacitance experiment geometry setup that we will explore in this paper.

1.1 Scanning Capacitance Experiments

The development of the scanning probe microscopy and electric field sensing techniques led to the discovery of the scanning capacitance microscopy. In the scanning capacitance experiments sharp metal tip (probe) is placed in close proximity to the surface of the sample. Due to electrostatic interaction between probe and sample we are able to sense the charges buried in the sample ([2],[3], and [4]). In other words charge accumulated in the sample, couples with the charge on the probe. Consequently capacitance of the system (probe-sample) is dependent of charge distribution on the sample (beneath the tip). So indirectly by measuring the capacitance of the system we are able to map the charge density along the sample. More amazingly this remote sensing technique allow us to measure charges buried beneath the sample surface. This technique helped us explore quantum mechanics of confined systems, and furthermore facilitate development of future generation of nano-electronic devices

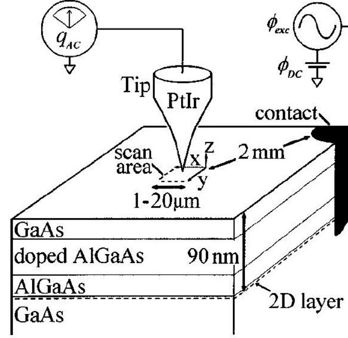

Figure 1-1: Schematic of the scanning capacitance microscopy experiment. The charges on the probe and 2D layer couple dictating the system capacitance, which allow us image charge distribution in the 2D layer [1].

[1].The actual setup of scanning capacitance microscopy is shown on the Fig. 1-1.

1.2 Two Dimensional Electron Gas (2DEG)

In this chapter we will give a brief review on the two dimensional electron gas systems. 2DEG system is heterostructure in which electrons are confined in a plane. Heterostructures are semiconductors assembled of different materials. The heterostructure modelled in this paper was $GaAs - Al_xGa_{x-1}As$. The common production technique is Molecular-beam Epitaxy where different semiconductor layers are grown on top of each other. Due to different properties like conduction and valence of different semiconductor materials, as we grow semiconductor layers we alter the valence or conductance of the heterostructure profile along vertical axis. Usually the lower valence material is an n-doped semiconductor. The excess electronic density created by doping flows toward the region of higher valence. The high-valence material acts like sink for the excess electrons of n-doped semiconductor. While crossing to the low energy region electrons lose extra energy and stay trapped in potential well. So at the end of the day we will end up with electrons trapped in potential well, that is the high valence layer. By narrowing the width of potential well we can restrict motion of electrons in z-axis, producing 2DEG [5].

The heterostructure modelled in this paper is shown on Fig. 1-2a. The system

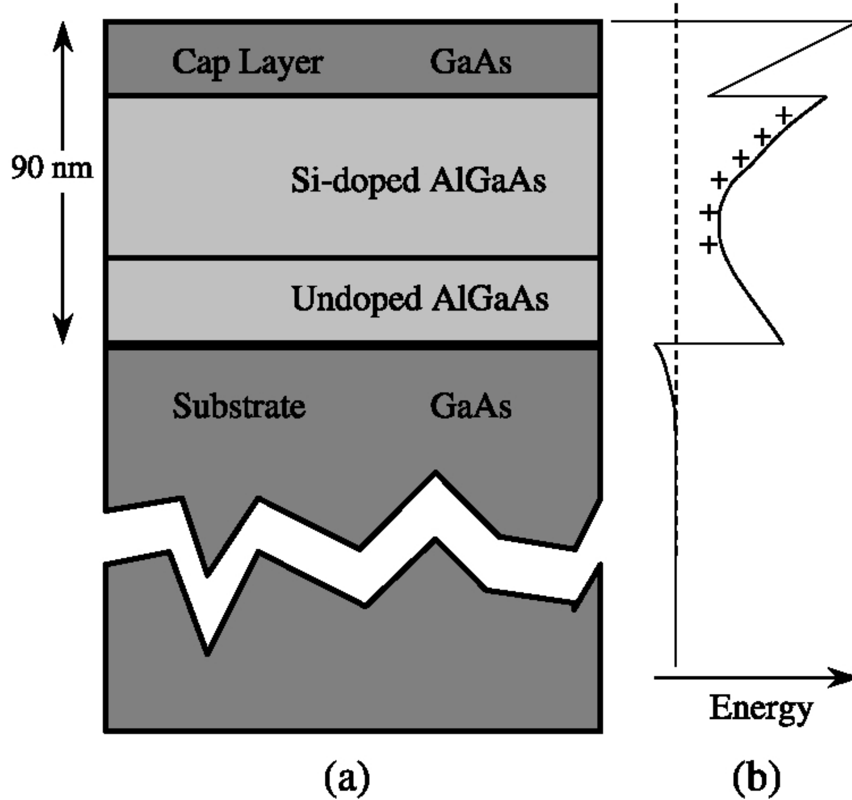

Figure 1-2: (a) The heterostructure geometry modelled in this paper, 2DEG is on the interface of undoped-$AlGaAs$ and $GaAs$, and is separated by $20nm$ from excess electron region of Si-doped $AlGaAs$; (b) Conductance profile of the heterostructure used in the simulation [6].

was grown on the $GaAs$ substrate, on top of it we have layer of undoped $AlGaAs$, followed by Si-doped $AlGaAs$, and finally cap layer was $GaAs$. This arrangement of the layers along vertical axis produces conduction band shown on Fig. 1-2b. The excess electrons from the Si-doped $AlGaAs$, flow into the region of the interface $GaAs$/undoped-$AlGaAs$ where they stay trapped in the narrow triangular quantum well, producing 2DEG.

1.3 Quantum Hall Effect

The classical Hall effect was discovered by Dr. Edwin Hall in 1879. If magnetic field is applied perpendicularly to the current flow in semiconductor (or metal) the

voltage difference is build up along the direction perpendicular to the both current flow and magnetic field (direction $\hat{k}$). The Hall effect is caused by discrete nature of current flow. Current is composed of electrons drafting in the current direction. Single electron experiences magnetic field force along $\hat{k}$ and therefore some electrons end up on the edges of the sample inducing voltage difference. Using the Hall effect one can measure charge carrier density of the sample by measuring Hall conductance. The conductance and charge density are connected by following formulae: $\sigma = \frac{nqc}{B}$, where σ - is Hall conductance, B is the magnetic field strength, n is the charge carrier density, q is the charge of unit carrier,and c is the speed of light).

In the 1982 Quantum Hall Effect was discovered. It was observed that in 2D systems of semiconductors and metals , for low temperatures (order of $350mK$) and high magnetic fields (around $1T$ and more), Hall conductance takes quantized values ($\sigma = \frac{\nu e^2}{h}$). The integer ν represents the Landau Level filling factor. If we express the charge density in function of ν and B we get, ($n = \frac{\nu eB}{hc}$. As we can see charge density is directly proportional to the Landau Level filling factor and strength of the magnetic field [7]. In this paper we will often refer to the magnetic field in terms of ν, and this is because ν has more intuitive meaning.

In our experimental setup we have 2D electron gas (2DEG) buried beneath semiconductor surface, on a low temperatures and high magnetic filed. The density profile of 2DEG will be quantized according to the Quantum Hall Effect. In our experiment we will explore properties of the Quantum Hall Liquid met in scanning capacitance microscopy experiments close to the integer filling factors.

1.4 Electrostatics of the complicated Geometry

The goal of this thesis is to build simulator capable of modelling complicated electrostatic geometries as one usually meets in scanning probe microscopy experiments [8],[2], and [3]. The geometry of the probe-sample model is shown on Fig. 4-1 and 1-1. The probe is in close proximity to the surface of the sample ($20nm$) , while the 2DEG is buried beneath $GaAs$ (90nm beneath sample surface). Top and bottom of

our model are defined as top and bottom metal gates, also boundary conditions were either metal boundaries or normal boundary conditions. Note that the setup on the picture is cylindrically symmetric along the Z axis. This geometry is fairly complicated and it's unsolvable analytically. To solve this and similar problems, often met in physics of 2DEG and Scanning Capacitance Spectroscopy one has to use numerical approach.

Therefore to solve electrostatic problems of 2DEG we had to develop electrostatic simulator. The simulator we developed is based on relaxation method and can model systems that are composed of vacuum, dielectric, metal, fixed charges, and semiconductor (of any reasonable density profile). Since the simulator is very flexible if would be easy to implement any additional material, if necessary. We solved electrostatics of the system for the potential distribution, from which all the other fields (electrostatic field, charge distribution) could be calculated. The basic algorithm of the relaxation method is following: entire system is represented by discrete material matrix, at each iteration every cell of the matrix is relaxed (potential is updated with better guess), and as we relax system finitely many times it should converge to the solution. One may ask how do we relax individual cell of the potential matrix? By using Gauss law applied to the discrete space we are able to calculate potential of the cell being relaxed in function of it's neighbors and other known parameters (dielectric constant, static charge or charge density), exact relaxation formulae is derived in next chapter.

In general things get a bit more complicated as we optimize the algorithm, and ensure convergence, but the idea of relaxation method is very simple. For the purpose of time/geomtry optimization we build two different electrostatic simulators , one was optimized for cylindrically symmetric systems and second one was was applicable arbitrary 3D system. the governing equations and algorithm of both simulators will be described in detail in the next chapter.

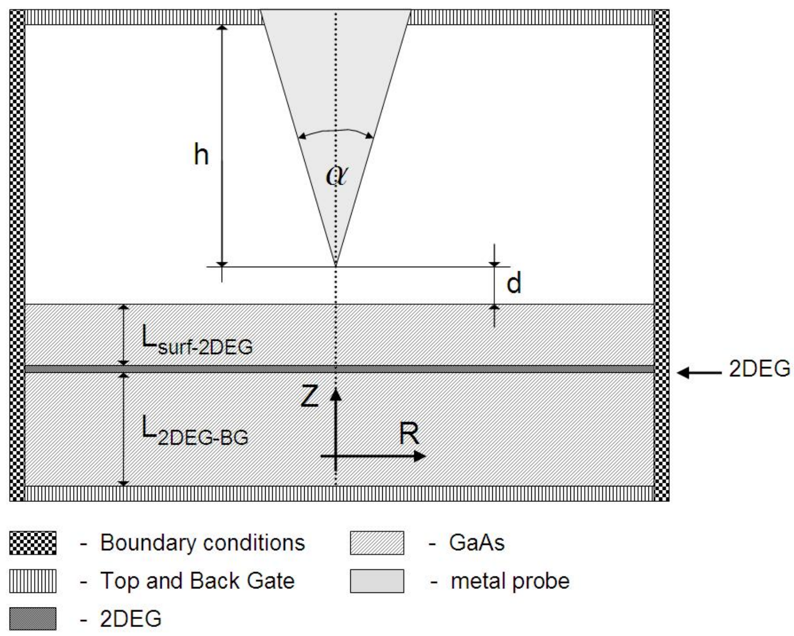

Figure 1-3: The geometry of the scanning probe above 2DEG.

Chapter 2

Simulation Details

As it was mentioned before, due to complexity of the system geometry we are unable to compute analytical solution, and therefore we had to solve it numerically. For this purpose we developed two electro-static simulators: one optimized for the cylindrically symmetric geometries and the other one for the arbitrary three dimensional systems. Both electro-static solvers were based on Successive Over Relaxation (SOR) technique [9]. The idea of Relaxation methods in general is to relax system for a number of iterations until it reach solution. In this chapter we will derive relaxation update equation from Gauss's law, for cylindrically symmetric systems as well as for regular 3D systems. In addition we will discuss convergence time of the simulation as well as convergence test criteria.

2.1 Poisson's Equation For Solving Electrostatics

Any electrostatic solver is actually Poisson's equation solver for a given geometry and initial conditions. The simulator was based on Poison equation solver. The Poisson's equation is given by Eq. 2.1.

$$\nabla^2 u(\vec{x}) = \frac{\rho(\vec{x})}{\varepsilon_r(\vec{x})\varepsilon_0}, \quad \text{Poisson's equation.} \tag{2.1}$$

Where u is the potential,ρ is the charge density, and ε_r is the relative dielectric

constat field.The equivalent to the Poisson's equation is the Gauss's law, which states that: "*total flux through any closed surface is equal to the sum of all charges inside divided by dielectric constant.*This can be written in the following form:

$$\Phi_s = \int_S \vec{E} d\vec{s} = \frac{\Sigma_S \ q}{\varepsilon_r(\vec{x})\varepsilon_0}, \text{ Gauss's equation.} \tag{2.2}$$

Where Φ_s is total flux through closed surface S, $\vec{E}$ is the electric field vector, $\vec{s}$ is the surface vector and, $\Sigma_S \ q$ is sum of all charges inside the S. We will derive relaxation equation from the Gauss's law because it's more intuitive, but the equations we will get are the equivalent to those derived using Poisons equation. Note that in Poisson's equation $\rho(\vec{x})$ is function of the position only. Since simulator supports semiconductor materials that actually have density function dependent on potential $\rho(\vec{x}, u)$ the problem gets nonlinear. In next chapter we will introduce the charge density function profiles of insulator, metals, and semiconductors.

2.2 Charge Density

Depending on the material we have different charge density functions. So for example in metal we have zero gradient of potential field which means that electrons inside the metal will rearrange their positions preserving the zero electric filed. In other words the zero electric field will maintain the constant potential of the metal cells. Opposite of metals are insulators (vacuum, dielectric). The charges are trapped in insulators, therefore the charge density in insulators remains constant at all times. Consequently the potential will adjust to the insulator so it's in agreement with Poisson's law. The charge density of the insulator in function of the potential is horizontal line since amount of charge in insulator is constant. The semiconductor are in between metals and insulators. In semiconductors the potential adjusts to to the charge density, but also charge density is now dependent on potential. In the Fig. 2-1 we can see semiconductor in function of the potential (dashed line). In absence of the magnetic field charge density is linearly decreasing function of the potential, but as we apply

large magnetic field the Quantum Hall take effect important. In sufficiently strong magnetic fields and low temperatures charge density in function of potential looks like the multiple step function (2-1). Since the step function is infinitely sharp, the first derivative of the charge density is delta function. However in real life the delta function is Lorentzian with finite width. For the purpose of simulating the semiconductor in magnetic field we approximate Lorentzian to the constant with a finite width. This assumption helped us improve the stability of the code with no lose of generality. This is because the shape of step jump, as long as it's reasonable, does not play crucial effect on 2DEG charge profiles. Finally the charge density function we used in simulation is shown on the Fig. 2-1. Note that depending on material we could have depletion density ρ_0 which represented the maximal electron depletion in the material. For the linear charge density dependence the slope corresponds to the density of states ($DOS = \frac{\partial \rho}{\partial u} = \frac{1}{\rho}\left(\frac{\partial n}{\partial E}\right)$). For the charge density profiles in magnetic fields the slope of the "step" was ten times greater than the DOS. And finally to conclude:

Metal: $u = const \ \Rightarrow \ \rho(u) =$ adjusts to anything.

Insulator: $\rho(u) = const \ \Rightarrow \ \ u =$ adjusts to anything.

Semiconductor: $\rho(u) = \rho_0 - u\ DOS, (B = 0)$ or the step function $(B \neq 0)$.

2.3 Deriving the Relaxation Equation

In this chapter we will derive relaxation equation. Depending on the type of the material the relaxation equation applied to the individual grid cell is different. The metal cells were held on constant potential (defined by the initial conditions). The relaxation of the dielectric, free space and semiconductor cells is a more complicated and can be derived using Gauss's law. In this chapter we will derive relaxation equation for the non-uniform grid spacing for both cylindrically symmetric and arbitrary three dimensional systems. The boundaries in our simulation were defined by normal

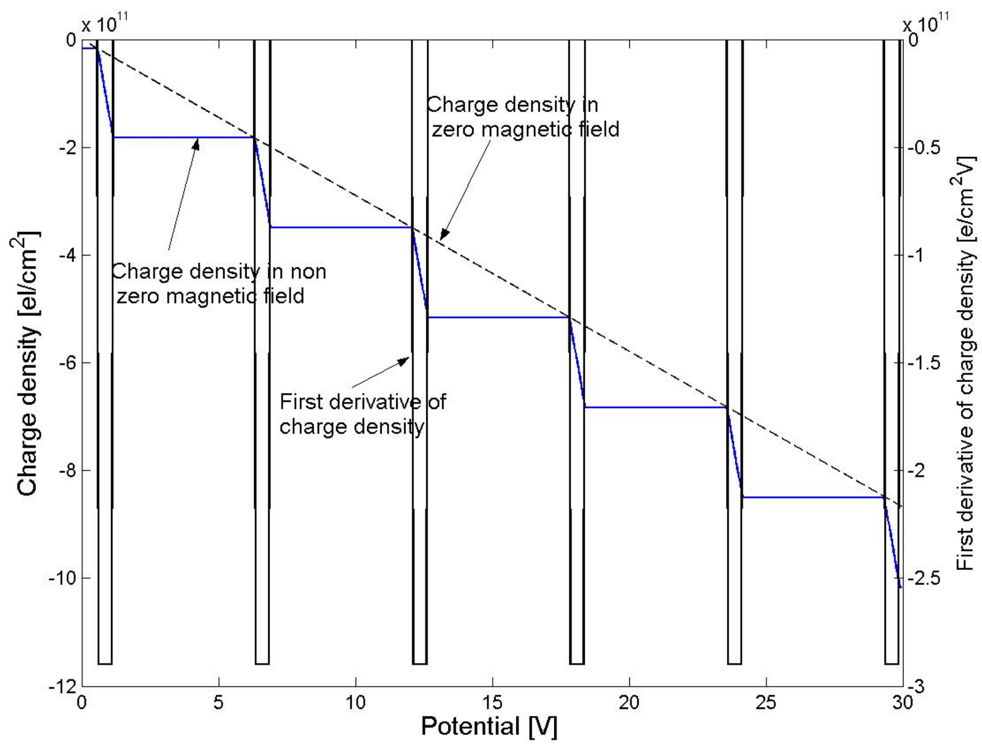

Figure 2-1: Charge density in semiconductor in function of the voltage.

boundary conditions (NBC) or fixed potentials (metal boundaries). Normal boundary conditions impose zero potential gradient in chosen direction, so for example if we have Material cell $M[i][j][ZMAX] = NormalBoundaryConditions$ it means that in each relaxation step we set it's potential to the potential of neighbor cell in chosen direction. In other words, $U[i][j][ZMAX] = U[i][j][ZMAX - 1]$, will assure zero electric field along $\hat{z}$ axes. Note that convergence time of the simulation is correlated to the type of boundary conditions we use. So for example simulation with metal boundaries converge much faster than the simulation where we have normal boundary conditions. Intuitively this is because metal boundary conditions are source of the exact potential therefore they emit information while NBC are patched by neighbors potential.

While deriving the relaxation equation we have to account for the charge induced by semiconductor which is defined by charge density function , $\rho = f(u)$. Let's call the initial value of the potential $u = U[i][j][k]$ and improved potential (the potential after single relaxation step) $u^* = U^*[i][j][k]$. In order to derive explicit relaxation equation, the charge density induced by potential in semiconductor is approximated to the first order Taylor expansion(Eq. 2.3).

$$\rho(u^*) = \rho(u) + \rho'(u)(u^* - u) \tag{2.3}$$

.

Using Taylor expansion we can derive explicate relaxation equation, but still maintain good approximation for the ρ reducing the numerical instability.As we will see this approximation is good enough and simulation is stable for a reasonable $\rho(u)$ functions. For the both cylindrically symmetric and 3D simulators system was described by material matrix M, relative dielectric constant matrix E_{rel}, potential matrix U and the matrix of the residual charges F.

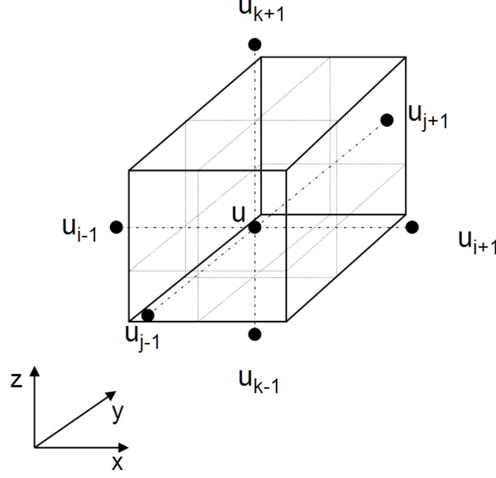

Figure 2-2: Schematics representation of the point relaxed in the three dimensional grid and it's nearest neighbors.

2.3.1 3D relaxation equation

In this section we will derive relaxation equation of the arbitrary 3D geometry. In this derivation we will assume that system has non uniform grid spacing given by X, Y and Z matrix, where spacial coordinate of (i, j, k) is given by (X[i][j][k],Y[i][j][k],Z[i][j][k]). All ofthe space metreces are monotonically increasing functions of indexes i, j and k. However this grid spacing has the following constrain:

$$\forall(i_1, j_1, k_1), (i_2, j_2, k_2) \begin{cases} i_1 = i_2 \Rightarrow & X[i_1][j_1][k_1] = X[i_2][j_2][k_2]; \\ j_1 = j_2 \Rightarrow & Y[i_1][j_1][k_1] = Y[i_2][j_2][k_2]; \\ k_1 = k_2 \Rightarrow & Z[i_1][j_1][k_1] = Z[i_2][j_2][k_2]. \end{cases} \tag{2.4}$$

This grid spacing setup allow us to derive simple relaxation equation and still be able to simulate relatively big systems that have interesting features in the areas that are few orders of magnitude smaller than the total system size. Of course one might think that we can always use brutal force approach and make very dense uniform spacing , but for the practical purposes this is useless. For example to simulate system that is on the order of magnitude of $1mm$ and has interesting features (eg.

probe -sample distance) on the order of magnitude of $1\mu m$ we need to make grid with at least few thousand cells per dimension. This would mean that at each iteration we would need to relax order of hundred billion cells which is extremely time consuming. The schematics representation of the point and it's nearest neighbors is shown on Fig. 2-2. Notation that we use is following, the subindex represents the direction in which we deviate from currently relaxed point so if we relax point $U[i][j][k]$ we will call it u , and it's nearest neighbors in x, y and z direction instead of $U[i-1][j][k]$, $U[i+1][j][k]$, $U[i][j-1][k]$, $U[i][j+1][k]$, $U[i][j][k-1]$, and $U[i][j][k+1]$ we call simply u_{i-1}, u_{i+1}, u_{j-1}, u_{j+1}, u_{k-1} and u_{k+1}. Analogously notation we used for the X, Y, Z, and $Erel$ matrices. Also to make equations less confusing we used following notation

$$\Delta p_1 = \frac{1}{2}(p - p_{l-1}),\ \Delta p_2 = \frac{1}{2}(p_{l+1} - p),\ \Delta p = \Delta p_1 + \Delta p_2.$$

$$\text{Where } p\ \epsilon\{x, y, z\}, \text{and } l\ \epsilon\{i, j, k\}.$$

For relative dielectric constant we use following notation:

$$\varepsilon_{l\pm 1/2} = \frac{1}{2}(\varepsilon_{l\pm 1} + \varepsilon),\ l\epsilon\{i, j, k\}.$$

The equation is derived from Gauss law's Eq. 2.5, and flux equation applied on a discrete 3D matrix (Fig. 2-2). The flux through the single face is equal to the average electric filed perpendicular to it multiplied by it's surface ($\Phi = \varepsilon_{rel}\bar{E}\Delta S$). Following this we get that flux through faces along $\hat{x}$, $\hat{y}$, and $\hat{z}$ are given by Eq. 2.5 - 2.8.

$$\Phi = \frac{Q}{\varepsilon_0}, \text{Gauss's Law;} \tag{2.5}$$

$$\Phi_x = \varepsilon_{i+1/2}\left(\frac{u_{i+1} - u}{\Delta x_2}\right)\Delta z\Delta y + \varepsilon_{i-1/2}\left(\frac{u_{i-1} - u}{\Delta x_1}\right)\Delta z\Delta y; \tag{2.6}$$

$$\Phi_y = \varepsilon_{j+1/2}\left(\frac{u_{j+1} - u}{\Delta y_2}\right)\Delta x\Delta z + \varepsilon_{j-1/2}\left(\frac{u_{j-1} - u}{\Delta y_1}\right)\Delta x\Delta z; \tag{2.7}$$

$$\Phi_z = \varepsilon_{k+1/2}\left(\frac{u_{k+1} - u}{\Delta z_2}\right)\Delta x\Delta y + \varepsilon_{k-1/2}\left(\frac{u_{k-1} - u}{\Delta z_1}\right)\Delta x\Delta y. \tag{2.8}$$

For the cube shown on the Fig. 2-2 we see that total flux out of the cube is equal

to the sum of the fluxes in x, y , and z direction($\Phi = \Phi_x + \Phi_y + \Phi_z$). Using this and Eq. 2.5 - 2.8 we get:

$$\frac{Q}{\varepsilon_0 \Delta x \Delta y \Delta z} =$$
$$-u\left(\frac{1}{\Delta x}\left(\frac{\varepsilon_{i-1/2}}{\Delta x_1}+\frac{\varepsilon_{i+1/2}}{\Delta x_2}\right)+\frac{1}{\Delta y}\left(\frac{\varepsilon_{j-1/2}}{\Delta y_1}+\frac{\varepsilon_{j+1/2}}{\Delta y_2}\right)+\frac{1}{\Delta z}\left(\frac{\varepsilon_{k-1/2}}{\Delta z_1}+\frac{\varepsilon_{k+1/2}}{\Delta z_2}\right)\right)$$
$$+\frac{1}{\Delta x}\left(\frac{u_{i+1}\varepsilon_{i+1/2}}{\Delta x_2}+\frac{u_{i-1}\varepsilon_{i-1/2}}{\Delta x_1}\right)+\frac{1}{\Delta y}\left(\frac{u_{j+1}\varepsilon_{j+1/2}}{\Delta y_2}+\frac{u_{j-1}\varepsilon_{j-1/2}}{\Delta y_1}\right)$$
$$+\frac{1}{\Delta z}\left(\frac{u_{k+1}\varepsilon_{k+1/2}}{\Delta z_2}+\frac{u_{k-1}\varepsilon_{k-1/2}}{\Delta z_1}\right) \tag{2.9}$$

If the point relaxed is the fixed charge point in the dielectric we get the final equation:

$$A = \frac{1}{\Delta x}\left(\frac{u_{i+1}\varepsilon_{i+1/2}}{\Delta x_2}+\frac{u_{i-1}\varepsilon_{i-1/2}}{\Delta x_1}\right)+\frac{1}{\Delta y}\left(\frac{u_{j+1}\varepsilon_{j+1/2}}{\Delta y_2}+\frac{u_{j-1}\varepsilon_{j-1/2}}{\Delta y_1}\right)$$
$$+\frac{1}{\Delta z}\left(\frac{u_{k+1}\varepsilon_{k+1/2}}{\Delta z_2}+\frac{u_{k-1}\varepsilon_{k-1/2}}{\Delta z_1}\right);$$

$$B = \frac{1}{\Delta x}\left(\frac{\varepsilon_{i-1/2}}{\Delta x_1}+\frac{\varepsilon_{i+1/2}}{\Delta x_2}\right)+\frac{1}{\Delta y}\left(\frac{\varepsilon_{j-1/2}}{\Delta y_1}+\frac{\varepsilon_{j+1/2}}{\Delta y_2}\right)+\frac{1}{\Delta z}\left(\frac{\varepsilon_{k-1/2}}{\Delta z_1}+\frac{\varepsilon_{k+1/2}}{\Delta z_2}\right);$$

$$u^* = \frac{-\frac{Q}{\varepsilon_0 \Delta x \Delta y \Delta z}+A}{B} \tag{2.10}$$

The Eq. 2.13 seem to be fairly complicated since it's very general, but one of the simplification that follow for the uniform grid ($\Delta x_1 = \Delta x_2 = \Delta y_1 = \Delta y_2 = \Delta z_1 = \Delta z_2 = a$) and uniform dielectric constants, ε lead to:

$$u^* = -\frac{Q}{3a\varepsilon_r\varepsilon_0}+\frac{1}{6}(u_{i+1}+u_{i-1}+u_{j+1}+u_{j-1}+u_{k+1}+u_{k-1}) \tag{2.11}$$

Which intuitively makes sense since for the free space we get that of a single

grid point is the average of it's nearest neighbors. Derivation for the semiconductor cells is analogous to dielectric derivation except that now we have Q dependent on current potential of the cell relaxed. So using Eq. 2.9 and 2.3 , together with notation introduced for A and B we get:

$$Q = \Delta x \Delta y \Delta z \; \rho(u^*) = \Delta x \Delta y \Delta z \; (\rho(u) + \rho'(u)(u^* - u)) \tag{2.12}$$

now using this with Eq. $\Rightarrow$

$$\frac{1}{\varepsilon_0}(\rho(u) + \rho'(u)(u^* - u)) = -u^* B + A \tag{2.13}$$

and finally we get

$$u^* = \frac{A - \frac{\rho(u)}{\varepsilon_0} + \frac{\rho'(u)}{\varepsilon_0} u}{B + \frac{\rho'(u)}{\varepsilon_0}} \tag{2.14}$$

The Eq. 2.14 is the most general relaxation and can be applied to any material (insulator, conductor, and semiconductor) for a properly chosen function ρ.

2.3.2 2D cylindrically symmetric

One the problems we were interested to solve, was to find the dependence of 2DEG density profile, and system capacitance on, tip-sample separation. This system is cylindrically symmetric and the relaxation equation derived in previous section could be reduced to the two dimensional equation. In 2D Cylindrical Simulator we define spacing matrices Z and R. R matrix represents matrix of radial distance from the coordinate beginning which is in i=0, j=0, similarly Z matrix represents the height matrix. Analogously to the 3D case we have:

$$\forall (i_1, j_1), (i_2, j_2) \begin{cases} i_1 = i_2 \Rightarrow & R[i_1][j_1] = R[i_2][j_2]; \\ j_1 = j_2 \Rightarrow & Z[i_1][j_1] = Z[i_2][j_2]; \end{cases} \tag{2.15}$$

The schematic representation of the grid geometry used is shown on the Fig. 2-3. Due to radial symmetry we are able to reduce problem to two dimensions. So let apply Gauss's law to the grid cell shown on Fig. 2-3, with an arbitrary angular width

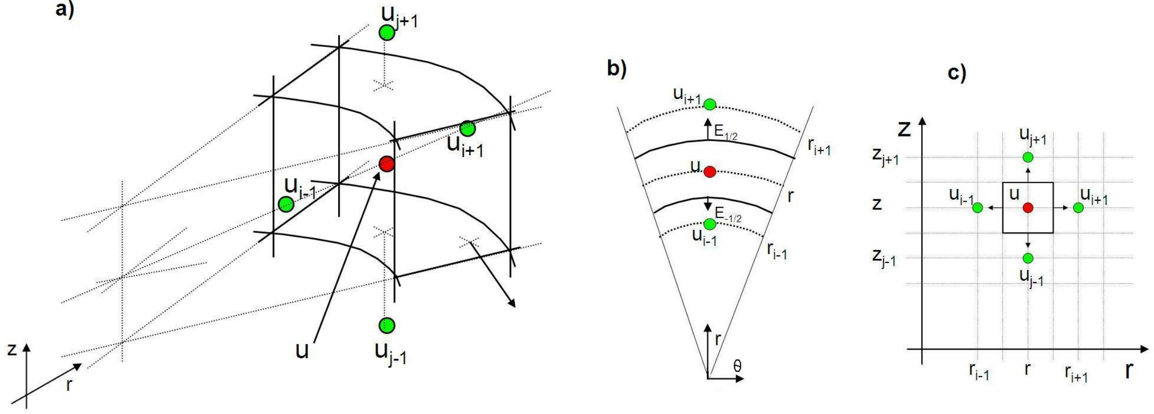

Figure 2-3: Schematics representation of the point relaxed in 2D cylindrically symmetric grid and it's nearest neighbors. a) the view from the side, b) top view c) side view representation of the grid

θ. The flux through the face of the grid cell can be defined as : $\Phi = \varepsilon_{rel}\ \Delta S\ \bar{E}$, (ε_{rel} - relative dielectric constant on the face, ΔS - the face surface, $\bar{E}$ - the mean electric field incident to the face. Then the fluxes out of the grid cell along $\hat{r}$,$\hat{\theta}$, and $\hat{z}$ are given by:

$$\Phi_r = \varepsilon_{i-1/2}\ \Delta z\ \theta r_{i-1/2} \left(\frac{u_{i-1} - u}{\Delta r_1}\right) + \varepsilon_{i+1/2}\ \Delta z\ \theta r_{i+1/2} \left(\frac{u_{i+1} - u}{\Delta r_2}\right), \tag{2.16}$$

$$\Phi_\theta = 0, \text{(due to cylindrical symmetry)}, \tag{2.17}$$

$$\Phi_z = \varepsilon_{j-1/2}\ \frac{\theta}{2\pi}\ (r_{i+1/2}^2 - r_{i-1/2}^2)(\frac{u_{j+1} - u}{\Delta z_1}) + \tag{2.18}$$

$$\varepsilon_{j+1/2}\ \frac{\theta}{2\pi}\ (r_{i+1/2}^2 - r_{i-1/2}^2)(\frac{u_{j-1} - u}{\Delta z_2}).$$

The total flux out of the cell is equal to the sum of fluxes along $\hat{r}$,$\hat{\theta}$, and $\hat{z}$. Also according to Gauss's theorem the flux is proportional to the charge enclosed by cell's surface. Since we are dealing with cell of arbitrary θ, we will not define cell charge but rather cell's charge density. Therefore $Q = \frac{\theta}{2\pi}\Delta z\ (r_{i+1/2}^2 - r_{i-1/2}^2)\rho$. In our derivation we will use analogous notation introduced subsection 2.3.1. Using charge definition with Gauss's law and flux definitions (plus dividing both sides of Gauss's law with θ) we get:

$$
\begin{aligned}
&\frac{1}{2\pi\varepsilon_0}\Delta z\ (r_{i+1/2}^2 - r_{i-1/2}^2)\ \rho = \\
&-u\left(\frac{\varepsilon_{i+1/2}\ \Delta z\ \ r_{i+1/2}}{\Delta r_2} + \frac{\varepsilon_{i-1/2}\ \Delta z\ \ r_{i-1/2}}{\Delta r_1} + (\frac{\varepsilon_{k-1/2}}{\Delta z_1} + \frac{\varepsilon_{k+1/2}}{\Delta z_2})\frac{1}{2\pi}\ (r_{i+1/2}^2 - r_{i-1/2}^2)\right) \\
&+\varepsilon_{i-1/2}\ \Delta z\ r_{i-1/2}\frac{u_{i-1}}{\Delta r_1} + \varepsilon_{i+1/2}\ \Delta z\ r_{i+1/2}\frac{u_{i+1}}{\Delta r_2} \\
&+ \frac{\varepsilon_{j-1/2}}{2\pi}\ (r_{i+1/2}^2 - r_{i-1/2}^2)\frac{u_{j+1}}{\Delta z_1} + \frac{\varepsilon_{j+1/2}}{2\pi}\ (r_{i+1/2}^2 - r_{i-1/2}^2)\frac{u_{j-1}}{\Delta z_2}
\end{aligned} \tag{2.19}
$$

If we define:

$$
\begin{aligned}
C &= \frac{\varepsilon_{i+1/2}\ \Delta z\ \ r_{i+1/2}}{\Delta r_2} + \frac{\varepsilon_{i-1/2}\ \Delta z\ \ r_{i-1/2}}{\Delta r_1} \\
&+(\frac{\varepsilon_{k-1/2}}{\Delta z_1} + \frac{\varepsilon_{k+1/2}}{\Delta z_2})\frac{1}{2\pi}\ (r_{i+1/2}^2 - r_{i-1/2}^2);
\end{aligned}
$$

$$
\begin{aligned}
D &= \varepsilon_{i-1/2}\ \Delta z\ r_{i-1/2}\frac{u_{i-1}}{\Delta r_1} + \varepsilon_{i+1/2}\ \Delta z\ r_{i+1/2}\frac{u_{i+1}}{\Delta r_2} \\
&+ \frac{\varepsilon_{j-1/2}}{2\pi}\ (r_{i+1/2}^2 - r_{i-1/2}^2)\frac{u_{j+1}}{\Delta z_1} + \frac{\varepsilon_{j+1/2}}{2\pi}\ (r_{i+1/2}^2 - r_{i-1/2}^2)\frac{u_{j-1}}{\Delta z_2}.
\end{aligned} \tag{2.20}
$$

For the fixed charge density in space we get:

$$
u^* = \frac{-\frac{1}{2\pi\varepsilon_0}\Delta z\ (r_{i+1/2}^2 - r_{i-1/2}^2)\ \rho + D}{A}. \tag{2.21}
$$

But if the relaxed cell is semiconductor then using the Eq. 2.3 and notation from Eq. 2.20 we get:

$$
\frac{\rho(u^*)}{\varepsilon_0} = \frac{1}{\varepsilon_0}(\rho(u) + \rho^{'}(u)(u^* - u)), \tag{2.22}
$$

Substituting this in Eq. 2.19 we get:

$$
\frac{1}{2\pi\varepsilon_0}\Delta z\ (r_{i+1/2}^2 - r_{i-1/2}^2)\ (\rho(u) + \rho^{'}(u)(u^* - u)) = -u^*\ C + D. \tag{2.23}
$$

And this finally leads to:

$$u^* = \frac{D - \frac{1}{2\pi\varepsilon_0}\Delta z\ (r^2_{i+1/2} - r^2_{i-1/2})(\rho(u) - \rho\text{'}(u))\ u}{C + \frac{1}{2\pi\varepsilon_0}\Delta z\ (r^2_{i+1/2} - r^2_{i-1/2})\rho\text{'}(u)}. \tag{2.24}$$

Now we are are ready to start iterating our system. In next subsection we will discuss relaxation algorithm and moreover we will focus on Successive Over Relaxation method.

2.4 Relaxation and Successive Over Relaxation

Most of the problems in physics are unsolvable analytically, therefore one needs to use numerical approach. In complex geometry systems (as one can meet in Ashoori's group experiments) we are not solvable analytically therefore we had to build electrostatical solver based on relaxation method.

The idea of the relaxation method is to iteratively improve guess, until we reach point at which the guess cannot be improved which means that we have converged to the solution. So, for example potential in every grid point can be expressed as a function of it's neighbors, such that it satisfies discredited Gauss's law, therefore the solution of the system is reached when all potential grid points simultaneously satisfy Gauss's law. The process of the relaxation is update of potential at each grid point in function of it's neighbors. So as we relax system we start to converge to the solution until we reach it.

As we mentioned before in our simulation we used Successive Over Relaxation method (SOR). So the basic idea is in to start relaxing our system with a given initial guess and as we relax our system we improve guess. And we keep relaxing system until we reach the solution. The relaxation algorithm is given below:

```
Initialize_System_Setup();
while (not converged)
{
    U’ = UpdateFunction(U);
    dU  = U’ - U;
```

```
    U = U  + SOR * \Delta U;
    Apply_Boundary_Conditions();
    F=Calculate_Residuals();
    Xi2 = sum of all F cells ;
    converged=Convegance_Test(Xi2);
}
```

As we can see at the beginning of each simulation we initialize geometry matrix and initial conditions, after what we start iterative relaxation. In each iteration we relax potential matrix (U) and calculate residual charge matrix (F). Each residual charge cell calculates how much electric charge in the cell is induced by numerical error. For example, ideally when system converges to the solution, free space cell we would have zero charge. By summing together squares of F matrix we obtain error which we call χ^2. Since we are dealing with computers and number have finite precision even in ideal case our χ^2 is not gonna converge to the zero but rather some number defined by data precision of our simulator and it's size. However as we converge to the solution we expect χ^2 converge to the steady constant. In order to accelerate convergence of the simulation we use over relaxation method where in each iteration step we calculate where U^* predicted by discretised Gauss's Law. And then to the updated potential we assign $U = U + \omega\Delta\ U$, where $\Delta U = U^* - U$ and ω is the over relaxation parameter (often call SOR). Reasoning for this will be discussed in a detail in the next section.

Depending on ω value we differ three different cases

$$\omega \begin{cases} > 1, & \text{over-relaxation;} \\ = 1, & \text{Gauss-Seidel;} \\ < 1, & \text{under relaxation.} \end{cases} \tag{2.25}$$

According to theorem SOR method is convergent only for $\omega \ \epsilon \ [0, 2]$ [9]. Moreover for $\omega \ \epsilon \ [1, 2]$, we get faster over relaxation than in the Gauss-Seidel case [9]. While for the $\omega \ \epsilon \ [0, 1]$ we get slower convergence. Running time comparison between Gauss-Seidel and over relaxation method will be discussed in next section.

2.5 Running Time Analysis

The running time of our simulator depends on the total number of points, n in our material matrix, in addition to the system size significant difference in running times is between classical relaxation and over relaxation algorithm. For regular relaxation we would have to relax $O(n)$ points per iteration, and system would converge in linear time, $O(n)$ iterations. Finally this would lead to the total convergence time of $O(n^2)$. While for the Successive Over Relaxation (SOR) we would spend $O(n)$ time for the single relaxation, while the time necessary to reach convergence was $O(n^{\frac{1}{2}})$, leading to the total time of $O(n^{\frac{3}{2}})$. Table of running times is shown on Table. 2.1. As we can see using SOR method we are able to speed up convergence by factor of $n^{\frac{1}{2}}$. The main reasoning such a significant difference between regular relaxation and SOR is that:

- *Relaxation smoothes only small fluctuations (nearest neighbors) $\rightarrow$ very slow propagation of the information through system.*
- *SOR works by creating "wave" like disturbances that propagate quickly to the edges $\rightarrow$ fast propagation of the information through system.*

	Relaxation	SOR
Single Relaxation Time	$O(n)$	$O(n)$
Convergence Time	$O(n)$	$O(n^{\frac{1}{2}})$
Total Time	$O(n^2)$	$O(n^{\frac{3}{2}})$

Table 2.1: Running time comparison of regular relaxation and successive over relaxation methods [10].

On the Fig. 2-4 we can see the distribution of the residual charge, at different iterations for successive over relaxation method used. Note that as we start iterating the wave like disturbances are created. This disturbances facilitate faster information propagation and therefore faster convergence. As we can see on the Fig. 2-4 (bottom-right picture) as we converge to the final solution wave like disturbances disappear and residual charge matrix looks like noise.

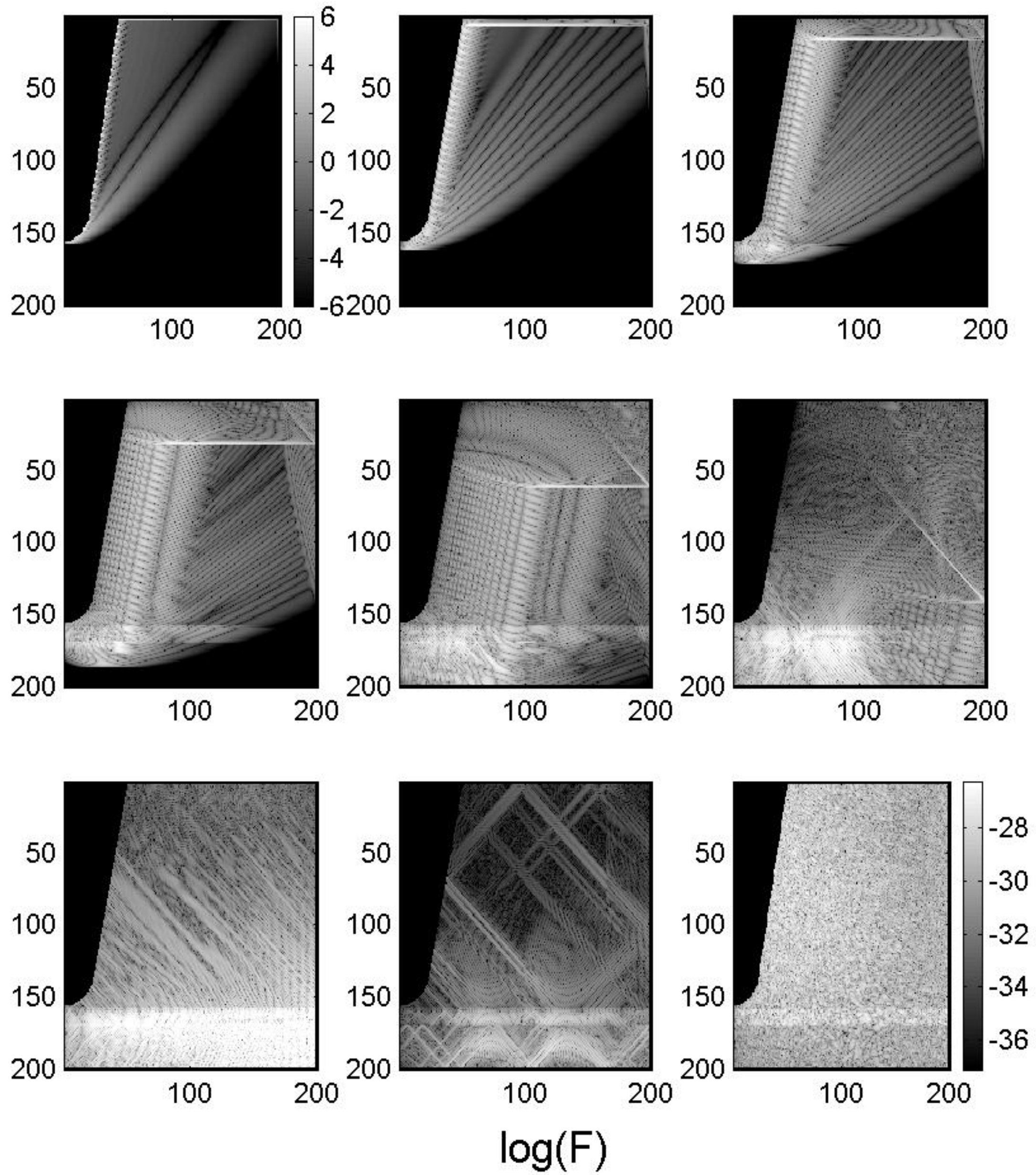

Figure 2-4: Snapshots residual errors for the 2D cylindrically symmetric systems for successive over relaxation. Snapshots were taken for iterations 1,5, 15, 30, 60, 140, 420, 900 and 2500 (starting from top-left and ending at bottom-right). We can observe wavelike disturbances and their propagation overtime.

2.6 "Adaptive" Successive Over Relaxation

In our simulator we were interested to simulate nonlinear systems often found in physics of 2DEG. Charge density in semiconductors is the function of it's potential, which is usually nonlinear dependence. Since even regular relaxation is not guaranteed to converge for non linear problems, we found the way to make our SOR simulator stable. The idea of our approach was to detect divergence in the system and as we detect it we try to restore stability, by dropping the SOR parameter in the region of the nonlinear $\rho(u)$ (call it SOR^*). The χ^2dependence on iteration number is shown on Fig. 2-5. Note on the figure the change in χ^2 after the iteration 501 and 865, in which divergence was detected and SOR^* has been readjusted (decreased by factor of around ~ 1.2) . For both readjustments χ^2 start converging again. Finally at the end of the day we successfully converge in finitely many iterations. In next subsection we will discuss how do we detect, ultimate convergence.

2.7 When do we stop iterating?

In this subsection we will discuss what criteria we used to terminate iterating. The idea of the relaxation methods is to iterate system until it reaches solution. As we relax our system we decrease systematic error, and we continue process of relaxation until we reach error that is caused by truncation (ex. finite precision of double). The error in truncation on our F field looks like white the noise (Fig 2-4, bottom-right), with amplitude proportional to the potential in the given region. So for example if we have higher relative dielectric constant *epsilon* in a given region, we can expect higher charge residuals. All this comes form the definition of the residual charge $F = (\rho_{external} - \rho)$, where $\varepsilon \nabla^2(u) = \rho$. In general we defined χ^2 as sum of all F squares scaled to number of grid points relaxed,in other words: $\chi^2 = \frac{\sum_{k=0}^{n} F_k^2}{n}$, where n is number of grid cells relaxed. χ^2 has roughly same value for the truncation error limit. Depending of simulation geometry the final χ^2 would vary, but in general for the double precision truncation error was around $10^{-26} - 10^{-30}$.

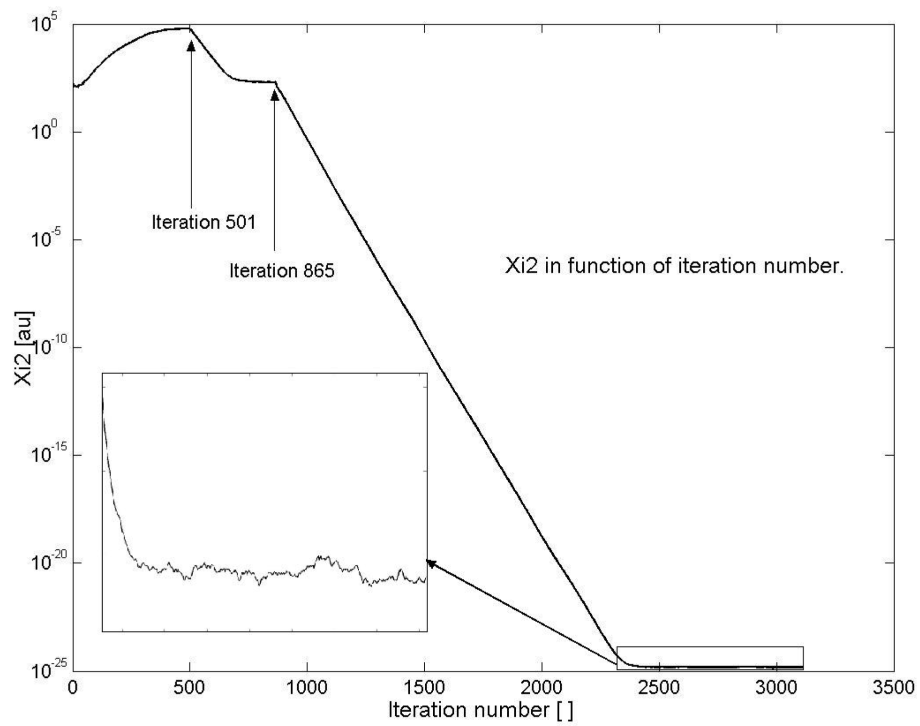

Figure 2-5: χ^2 in function of the convergance, for "adaptive" sucessive overrelaxation approach.

The algorithm we used to maintain stability and detect convergence in the simulator is shown below:

```
nIter =0; // number relaxations performed
while (not converged)
{
    relax(); // relax system
    if  ((nIter >500) and
        (Xi2[nIter] <Xi2[nIter-50]))  // if we notice Xi2 fluctuations
    then
    {  update_SOR*();  SOR_Steps++; // update nonlinear SOR
       if (SOR_Steps_To_Converge < SOR_Steps)
       then
             if  (Xi2[0] < Xi2[nIter]*10)
                converged = true;
    }
}
```

Our convergence criteria was following . In every iteration we would check if we have passed at least 500 iteration and if χ^2 value starts to oscillate or diverge in last 50 iterations. So if it is the case we readjust SOR* parameter in the region of nonlinear charge density. Further more we would check if we have made required number of SORsteps (around 6 works in general). If we did so we check if our current χ^2 has significantly converged compared to initial value and if it is the case we have converged successfully. This is shown in pseudo code syntax above.

Chapter 3

Results

Now since we are familiar with the simulation details we are ready to explore the results. In the first chapter we introduced the system geometry. The proximity of the tip and sample surface is usually held constant ($\sim 20nm$), in addition probe in the real had round tip. Unlike in the scanning tunnelling microscopy where we measure tunnelling current, in scanning probe technique there is no tunnelling current and we measure charge on the metal tip. Note that metal tip is in direct contact with top gate, which can induce unrealistic tip charge dependence on tip bias, because of probe - top gate coupling. In order to avoid this artifact instead of measuring tip capacitance we would measure sample capacitance. Charge induced on the tip is highly dependent on sample-tip proximity, bias voltage and tip shape, therefore our first simulation explored effects of tip shape and simple-probe distance on system capacitance (charge induced in the tip). After this we explored charge density profile induced in 2DEG for various magnetic fields. In addition we will observe quantum bubble and incompressible strip formation, for the magnetic fields close to the integer Landau level fillings. After this we will explore incompressible strip formation on the edges of the metal gate. Finally we will explore charge density profiles under the influence of the magnetic field of the sample with donors in magnetic field.

3.1 Tip Approach

In this experiment the goal was to determine dependence of tip capacitance on tip shape and tip-surface proximity. In all of the experiment the tip was held on constant bias voltage of $1V$. The top and bottom metal gates were grounded to $0V$ and top surface of bottom gate was covered with $0.1\mu m$ layer of dielectric with dielectric constant $E_{rel} = 13.0$. We record the tip capacitance in function of it's distance from the dielectric surface. The capacitance was calculated by summing the total charge on the metal tip surface and dividing it by the tip bias voltage. The detail scheme of the system geometry used in this experiment is shown on figure Fig. 3-1. The grid resolution we used was around 400×400.

The main goal of this experiment was to get qualitative insight of tip capacitance dependence on tip shape. All of the tip capacitances showed on Fig. 3-2 are normalized by division with capacitance at the biggest tip-dielectric surface separation. Therefore all the capacitances end at relative capacitance 1.00, in addition we offseted each consequent capacitances by 0.002 for the easier view. As we can see the sharp tip shows the steadiest capacitance dependence of the tip-surface separation. Also the relative capacitance for the separations less than $0.2\mu m$ is very steep function. This specific length is mainly on the order of dielectric thickness and in a way represents the resolution of our microscope. Also from Fig. 3-2 we can conclude that the wider tip we have the steeper dependence it is. Finally for the round tip we have far more stepper capacitance dependence than when the tip is flat. The results obtained by simulation qualitatively match with results from the real experiment, but any quantitative comparison would be very complicated.

3.2 Quantum Bubble Formation

The main goal of this part of the experiment was to capture evolution of the 2DEG charge density under the influence of tip voltage change. The experiment was carried out for magnetic field $\nu = 0.9$ where the tip voltage was varied from 0 to $+2V$, and

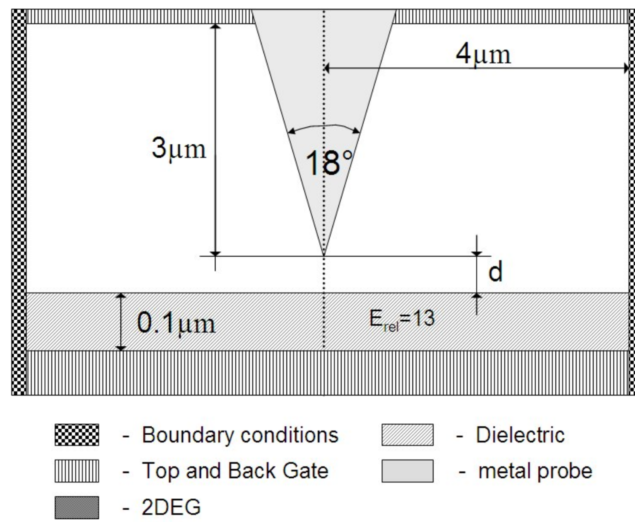

Figure 3-1: Scheme of geometry setup for the tip approach experiment.

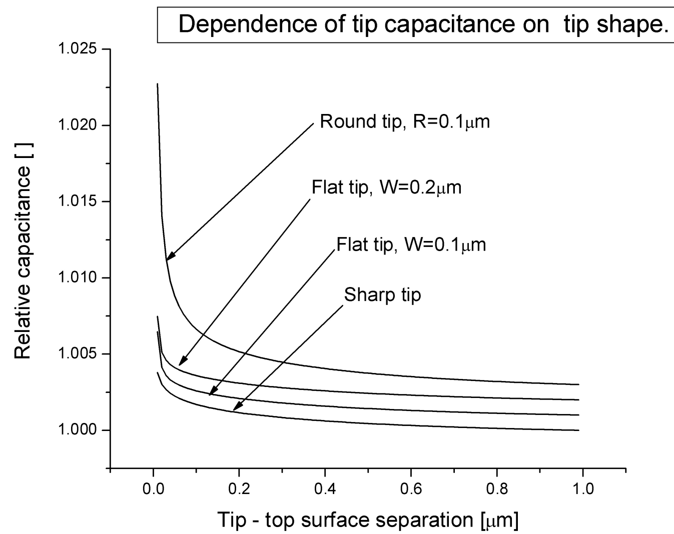

Figure 3-2: Dependence of relative tip capacitance on the tip shape.

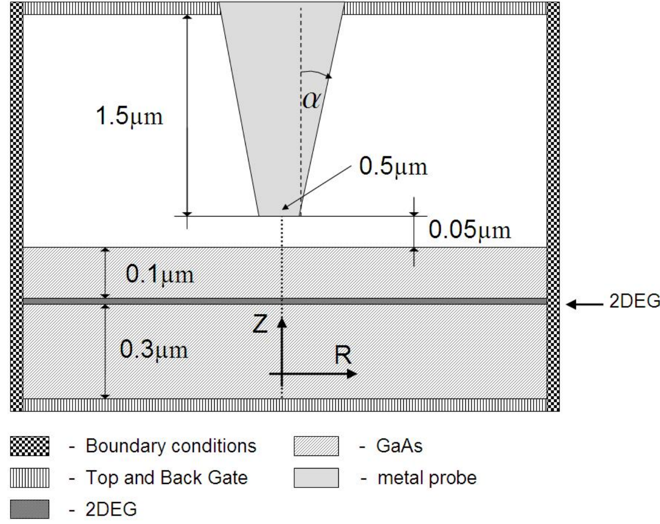

Figure 3-3: Scheme of geometry setup for the bubble formation experiment.

$\nu = 1.1$ where tip voltage was varied from 0 to $-2V$. In both cases the geometry setup was equivalent and is shown on Fig. 3-3. The tip was flat with width of $0.5\mu m$,tip half angle α was 9^0, 2DEG was buried around $0.1\mu m$ under the top surface of $GaAs$ dielectric with dielectric constant $Erel = 13.0$.

3.2.1 Quantum Bubble Inflation ($\nu = 0.9$)

In this experiment we observed origin and inflation of the quantum bubble. The experiment was carried out at magnetic field $\nu = 0.9$, while tip voltage was varied between $0.00V$ and $+2.00V$. On the Fig. 3-4 the formation of the quantum bubble is shown. The electrons in bubble occupy the filling Landay level $\nu > 1.00$, and bubble is separated from rest of the 2DEG ($\nu < 1.00$) by incompressible strip corresponding to the integer Landay level filling factor. As we can see from the Fig. 3-4 initially when the tip voltage is relatively small $0 - 0.24V$ we have no bubble, but once we go over the $0.28V$ the bubble is formed, with further increase of the tip-bias more electrons are attracted by tip's positive potential and the electron density raises leading to the expansion of the quantum bubble. Additionally since in the real experiment we do not capture 2DEG charge distribution directly, but through the system capacitance

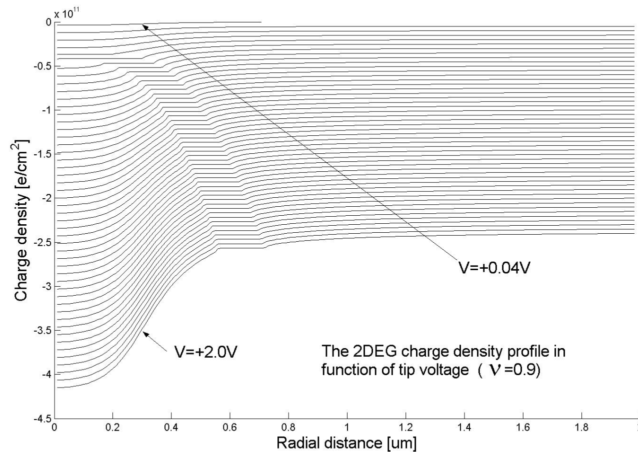

Figure 3-4: Quantum bubble formation for $\nu = 0.9$. (Note: the consequent charge densities are offseted by $-10^{10}e/cm^2$.)

change. Therefore we were interested to capture system capacitance dependence on tip bias, Fig. 3-5. In this simulation run the system capacitance is defined as the sample capacitance. As we can see on Fig. 3-5 the system capacitance becomes extremely steep function of tip-bias as we go through the bubble formation. This means that with a minimal changes of the tip-bias we get large changes in the tip and sample charges. In other words that once the bubble is formed the electrons from 2DEG favor accumulating in the it. Furthermore the increased accumulation of electrons directly beneath the tip leads to sharp raise in system capacitance.

3.2.2 Quantum Bubble Depletion ($\nu = 1.1$)

The idea of this part of the experiment was to start with 2DEG in the ($\nu = 1$) Landay level and then, by applying more negative bias voltage to the tip we would deplete the 2DEG region beneath the tip, entering the lower Landay level ($\nu = 0$). So in this case we would form the bubble that lacks in electrons. Like in the previous experiment the bubble was separated by rest of the 2DEG by the incompressible strip. On the Fig. 3-6 we can see that initially ($V_{tip} = -0.1V$), entire 2DEG is in the $\nu = 1$, and then as we decrease voltage to the $V_{tip} = -0.2V$ the "anti" bubble is formed and the 2DEG directly beneath the tip enters the $\nu = 0$ zero Landay level separated by rest of the

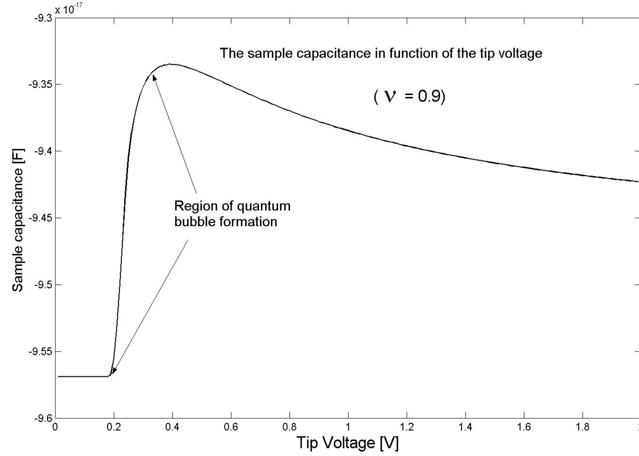

Figure 3-5: Sample capacitance in dependence of the tip bias. ($\nu = 0.9$)

2DEG by incompressible strip. If we decrease bias voltage furthermore, the bubble depletion expands and the radius of the incompressible strip raises. In addition we measured the system (sample) capacitance in function of the bias voltage. As we can see on the Fig. 3-7 the system capacitance becomes extremely steep function of the tip bias in regions in which the "anti" bubble has been just formed and starts to expand. Once the 2DEG has entered the lover Landay level the tip bias more effectively repels electrons from 2DEG beneath tip making the sudden changes in the tip capacitance.

3.3 Incompressible Strip Formation at the Meatal Gate Edge

In this simulation we were interested to capture the incompressible strip formation in 2DEG for the magnetic fields close to the integer Landau level fillings. In this setup we had metal gate on the surface of the undoped $GaAs$. The metal gate was covering only the left half of the system, and 2DEG was around $90nm$ below $GaAs$ top surface. Both top and metal gate of the system were grounded ($0V$) while metal gate had potential of $-42mV$, this potential is caused by difference of the chemical potential

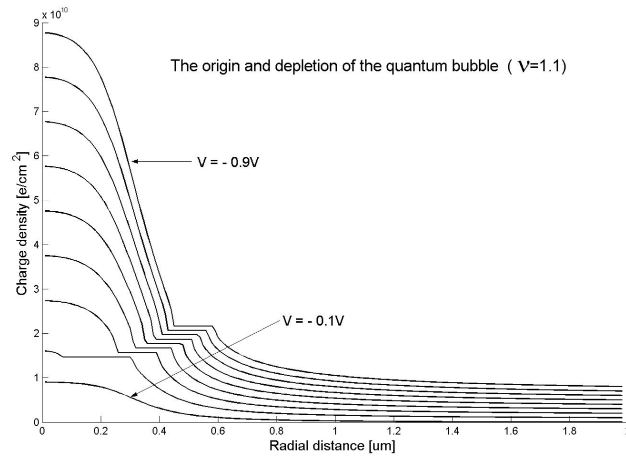

Figure 3-6: Quantum "anti" bubble formation for $\nu = 1.1$. (Note: the consequent charge densities are offseted by $-10^{10}e/cm^2$)

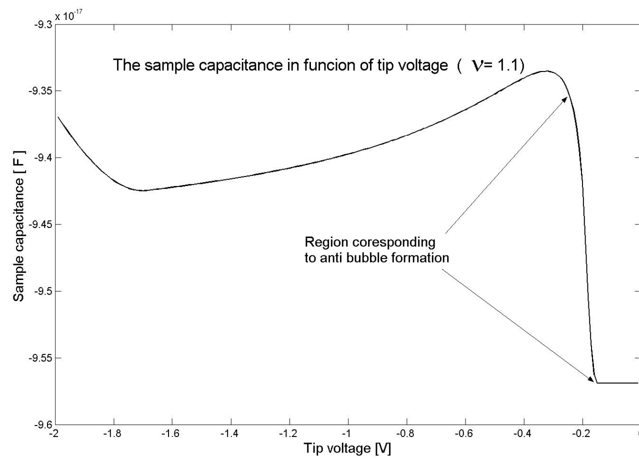

Figure 3-7: Tip capacitance in dependence of the tip bias. ($\nu = 1.1$)

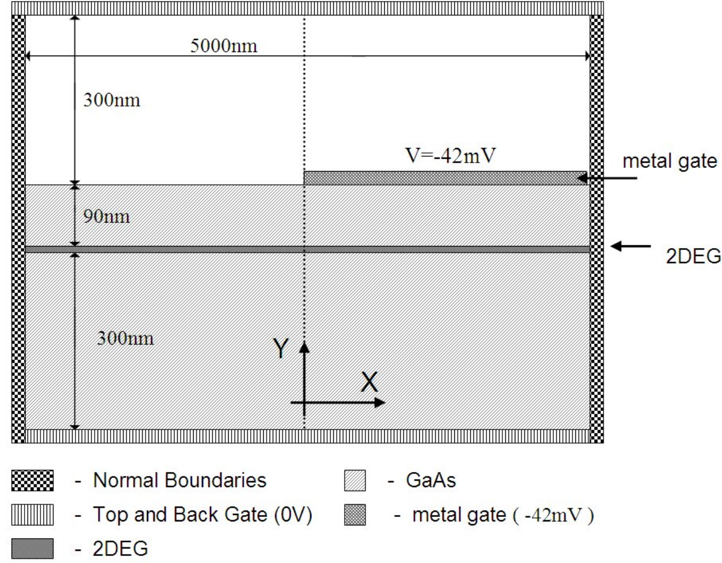

Figure 3-8: Schematics of the metal gate edge simulation.

of Zn gate and 2DEG. Top gate was placed around $300nm$ above $GaAs$ surface while the bottom gate was $300nm$ below the 2DEG. the schematic representation of the system setup is system setup is shown on the Fig. 3-8.

The goal of this experiment was to explore 2DEG charge distribution near integer Landau Level fillings. Therefore we run simulation for magnetic fields of $\nu = 0.70 - 1.05$. The simulation results are shown on the Fig. 3-9. As we can see the electrons are pushed from the metal gate and in the right part of the system electron density is higher than in the left. For the $\nu = 0.85$ the electron density on the right of the system is overfilling the first Landau level and we observe strip formation on the metal edge. As we raise the electron density we can see that strip shifts to the left and finally when entire 2DEG is above $\nu = 1.00$ the strip disappears.

3.4 Donors in Magnetic Field

In this part of the experiment we used 3D simulator to obtain realistic distributions od the 2DEG systems often meet in Ashoori's group experiments. The basic geometry of the system is shown on the Fig. 3-10. As we mentioned in the introduction, the

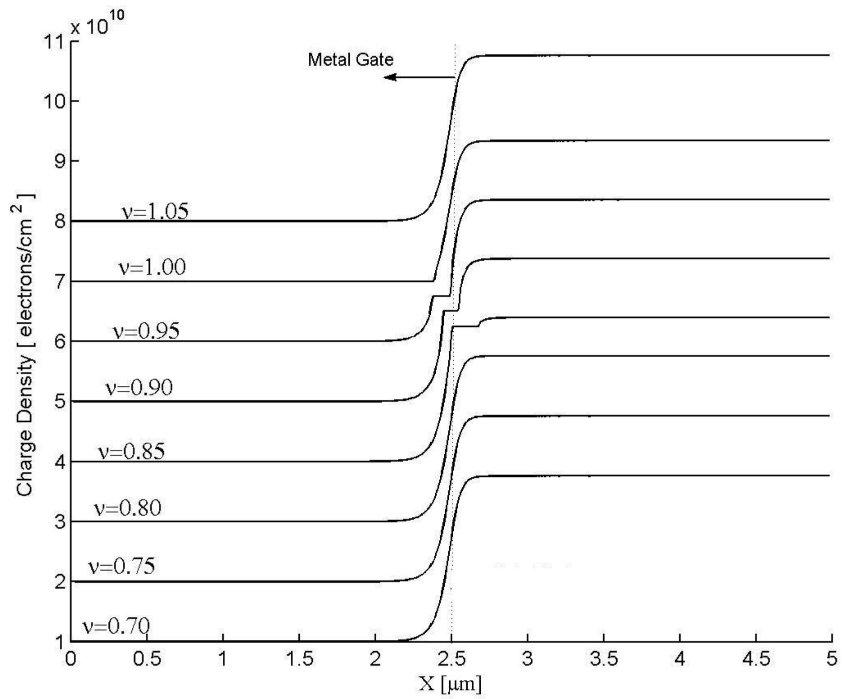

Figure 3-9: Electron density distribution for the metal gate edge simulation. Consequent distribution correspond to different Landau Level fillings (Magnetic field applied).Each distribution was offset by $10^{10} el/cm^2$ for clear view. We can see incompressible strip formation on the metal edge near integer Landau level fillings.

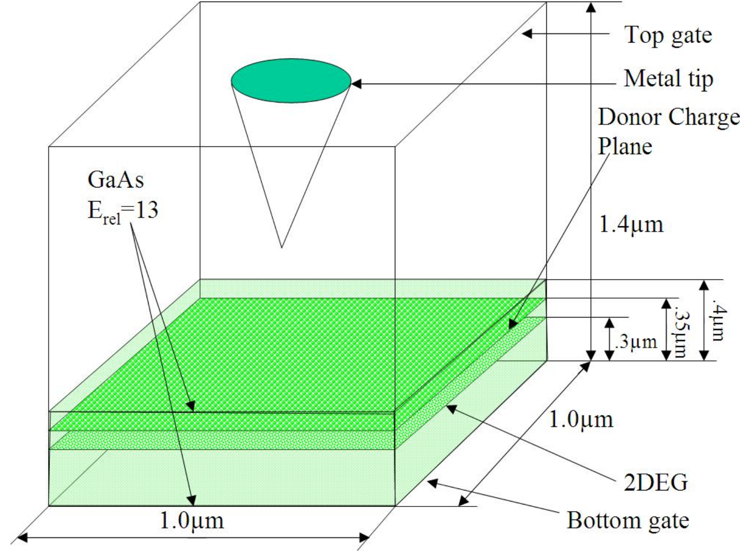

Figure 3-10: Schematics of the "donor's in magnetic field" simulations.

2DEG is trapped between layer of $GaAs$ and undoped $AlGaAs$ on top of which we have $Si-$doped $AlGaAs$ which is source of electron donors. The excess electrons go to the energetically more favorable region (2DEG plane), while transferring to 2DEG the electrons loose extra energy and stay trapped in 2DEG. This leaves the donor layer with randomly distributed positive charges at the Si donor spots. In our experiment the donor surface density is around 1.5×10^{11}donors/cm^2. Basically in this experiment we will explore influence of two different charge distributions on the 2DEG charge density profiles. First distribution assumes that each donor donates electron to the 2DEG, and we call this *point charge distribution*. The second distribution assumes that only 10% of the positive point charges are fixed in the donor layer, and that other 90% of positive charges are uniformly distributed through the donor plane, this distribution we call *"smooth" point charge distribution*. For the 2DEG profiles we use gray colormap which colors the white high density regions while the low density regions are colored black. In addition when edge was included for 2DEG profiles were colored by black ($\nu > 1.0$), gray ($\nu = 1.0$), and white ($\nu < 1.0$). This was done for easier view od incompressible strip (the gray region).

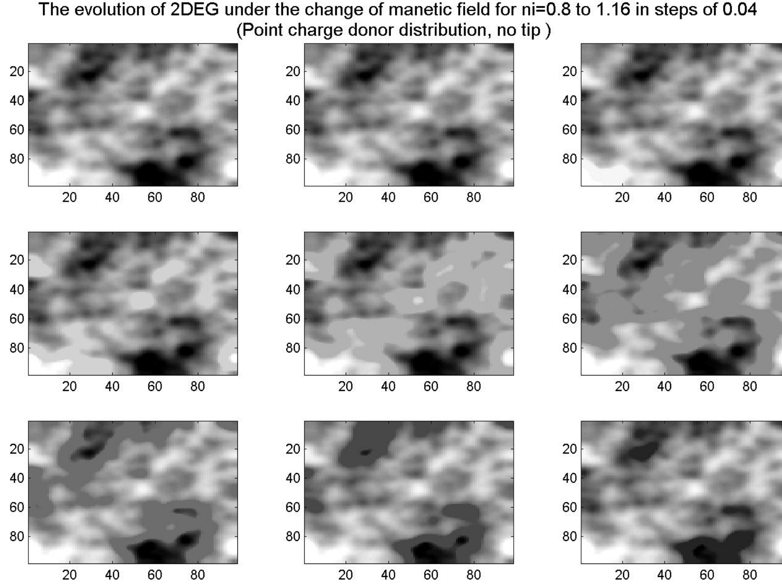

Figure 3-11: The evolution of 2DEG under the influence of magnetic field, for the point charge donor distribution.

3.4.1 2DEG charge density induced by donor layer

In this simulation we observe the 2DEG evolution with magnetic field change for a both "smooth" and regular point charge distribution in the donor layer. The 2DEG charge distribution in function of the magnetic field applied is shown on the Fig. 3-11. As we can see initially all the 2DEG is filling the Landau level $\nu = 0$, and 2DEG charge distribution is dictated by random donor distribution in upper layers. Then as we raise magnetic field some of the 2DEG starts to fill the upper Landau level, producing the regions of incompressible strip (the uniformly gray colored regions). Similar thing happens in case of "smooth" point charge distribution (Fig. 3-12) except that in this case the incompressible strips start to show for about $\Delta\nu = 0.2 - 0.3$ higher magnetic field. It's hard to give any quantitative comparison but in the case of the "smooth" point charge distribution it looks like it the incompressible strips are wider and more arc features on the strip edges can be observed.

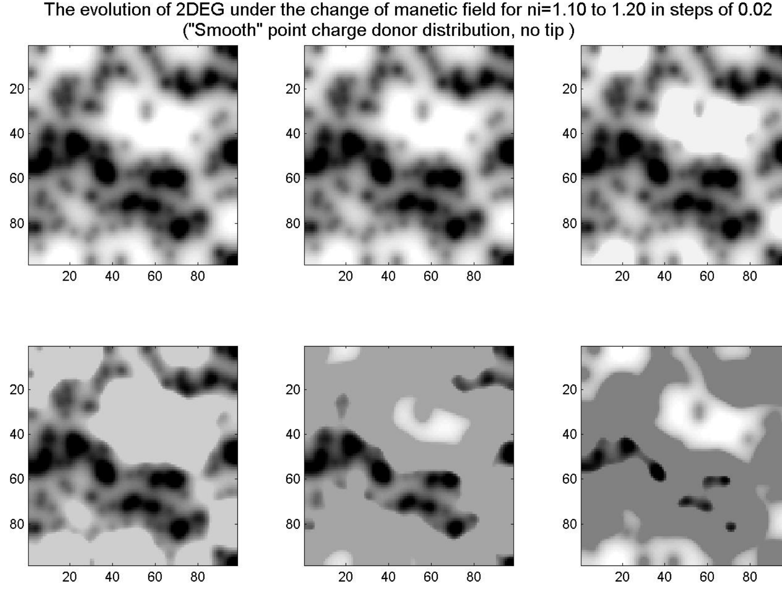

Figure 3-12: The evolution of 2DEG under the influence of magnetic field, for the "smooth" point charge donor distribution.

3.4.2 2DEG charge density induced by donor layer and metal gate edge

In this part of the simulation we were interested to explore evolution of 2DEG charge density profiles under the influence of magnetic field. We run simulations for both point and "smooth" and regular point charge distribution. The results are shown on the Fig. 3-13 and 3-14. For the both distributions we can observe that at the certain magnetic field the 2DEG in region beneath metal gate edge are separated by incompressible strip. This means that the 2DEG which is not under the metal gate enters the next Landau level before rest of the 2DEG. The incompressible strip along the metal gate edge is much more distinguishable in the case more realistic "smooth" point charge distribution. Also incompressible strip stays in close proximity to the metal edge never extending further that $0.1\mu m$ from the edge. Interestingly we can observe the arc features along the strip which are caused by point charges in the donor level.

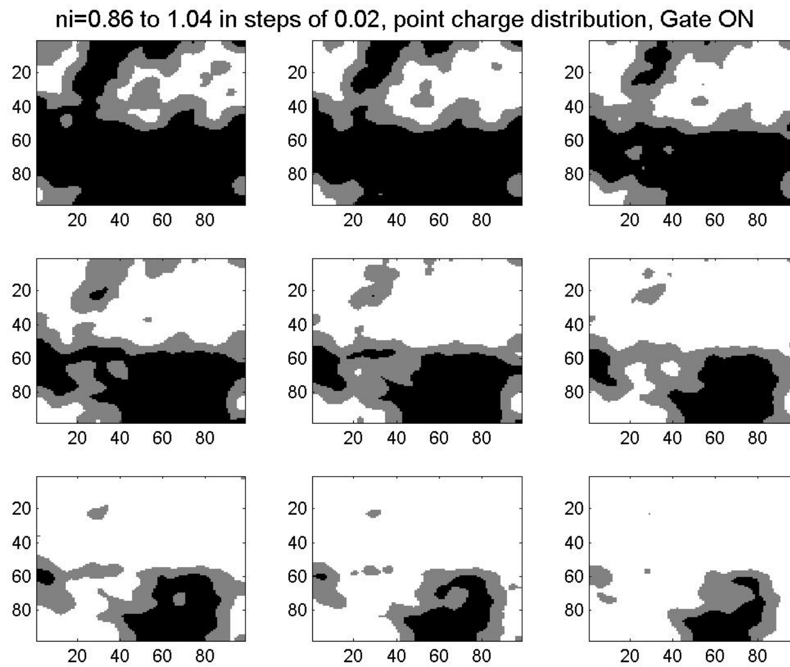

Figure 3-13: The evolution of 2DEG beneath the metal edge under the influence of magnetic field, for the "smooth" point charge donor distribution (black - $nu > 1.0$, gray - $\nu = 1.0$, and white - $\nu < 1.0$).

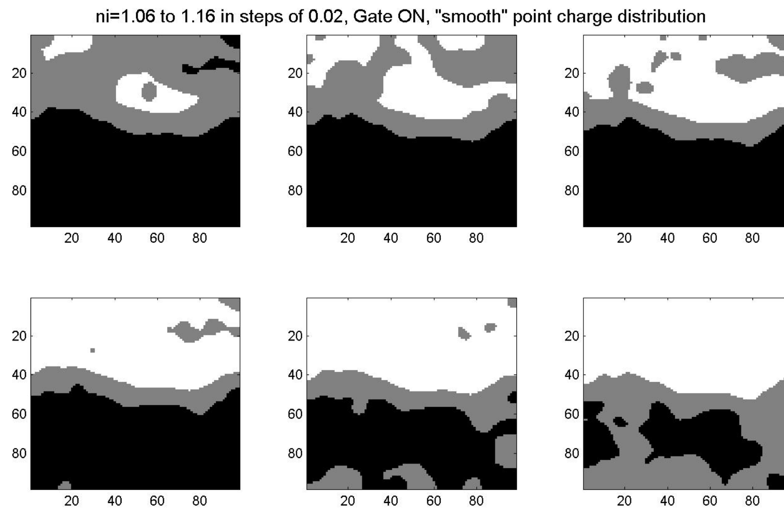

Figure 3-14: The evolution of 2DEG beneath the metal edge under the influence of magnetic field, for the "smooth" point charge donor distribution (black ($\nu > 1.0$), gray ($\nu = 1.0$), and white ($\nu < 1.0$).

Chapter 4

Summary

In this paper we presented the complex geometry electrostatic simulator. The simulator was based on Poisson's equation solver. For the purpose of better time/memory performance for the specific geometries we developed 2D simulator that was optimized for the cylindrically symmetric geometries and the 3D simulator that could be applied to arbitrary 3D geometries. Both simulators were based on the Successive Over Relaxation (SOR) technique. Once we include semiconductor to the simulation the problem becomes nonlinear, because semiconductor charge density is dependent on it's potentia. For nonlinear problems there is no guarantee that SOR converges. We maintained stability by introducing the SOR* parameter (which is SOR for nonlinear materials). Whenever we would detect instability in the simulator we would decrease SOR* by dividing it with SOR_{step} (usually $SOR_{step} = 1.2$). This worked perfectly fine and we were able to simulate nonlinear materials (semiconductors in magnetic field). Using the simulator developed we explored different properties of the metal probe - 2DEG interaction. First we explored properties of the tip shape on the tip capacitance. We saw that for the tip-dielectric surface distances greater few tip widths/radiuses, tip shape is not as relevant. For the close tip-sample proximities the tip capacitance becomes steep function and the wider tip it the steeper function we have. Finally the steepest dependence was observed for the rounded tip. We also explored the quantum bubble formation and depletion. In both cases the bubble was separated from rest of the 2DEG by the incompressible strip and origin of bubble

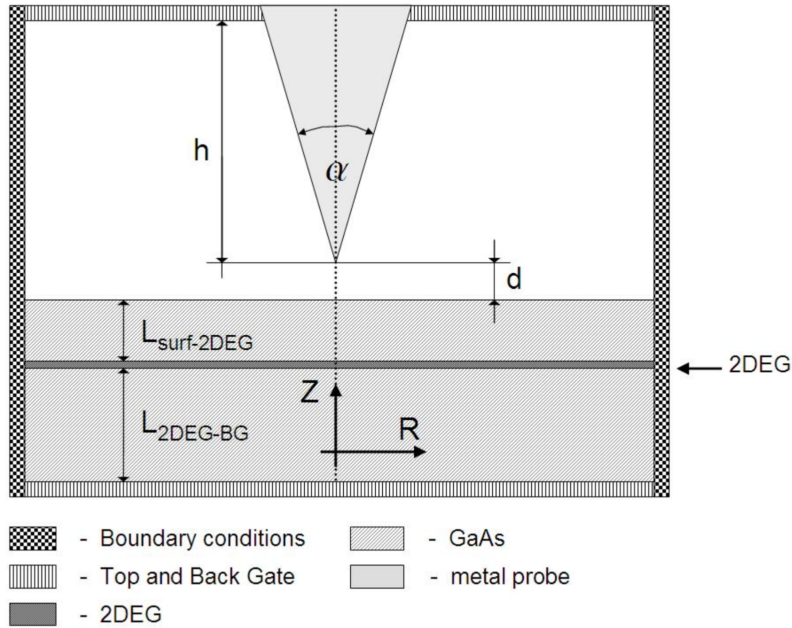

Figure 4-1: The geometry of the scanning probe above 2DEG.

formation/depletion was always followed by sharp changes of tip capacitance in function of tip bias. In addition we explored the incompressible strip formation at the metal edge, where it was noticed that the strip remains in close proximity ($\sim 0.1\mu m$) to the metal edge. Finally we explored the realistic 2DEG profiles induced by the positive point charges distribution in the donor layer of 2DEG heterostructure. We observed the 2DEG charge density evolution in function of the magnetic filed change for the point charge and "smooth" point charge distributions. We explored 2 different geometries one where metal gate edge was present and the other where we had no metal gate. The results obtained could be qualitatively compared to those obtained by experiment, while the "smooth" point charge would result much more realistic features. Finally the test examples we showed in the results chapter are just a examples of problems that we can solve using the simulators we developed. The simulators can be applied to the various other problems and I hope their robustness, speed, and flexibility will find while applications in further research of sub-micronic devices.

Bibliography

[1] P. I. Glicofridis S. H. Tessmer, G. Finkelstein and R. C. Ashoori. Modeling subsurface charge accumulation images of a quantum hall liquid. *Phys. Rev. B*, 66(125308):1+, September 2002.

[2] R. C. Ashoori L. N. Pfeiffer K. W. West N. B. Zhitenev, M. Brodsky. Localization-delocalization transistion in quantum dots. *Science*, 285:715+, July 1999.

[3] S. H. Tessmer R. C. Ashoori M.R. Melloch N G. Finkelstein, P. I. Glicofridis. Imaging of low compressibility strips in the quantum hall liquid. *Phys. Rev. B*, 61:16323, June 1999.

[4] P. I. Glicofridis S. H. Tessmer, G. Finkelstein and R. C. Ashoori. Subsurface charge accumulation imaging of a quantum hall liquid. *Nature*, 289:90+, July 2000.

[5] John H. Davies. *The Physics of Low-Dimensional Semiconductors: An Introduction*. Cambridge University Press, 1981.

[6] Paul I. Glicofridis. Phd thesis. Physics research, MIT, Physics Department, September 2001.

[7] David J. Griffiths. *Introduction to Quantum Mechanics*. Prentice Hall, 1994.

[8] R. C. Ashoori M. Shayegan Science G. Finkelstein, P. I. Glicofridis. Topographic mapping of the quantum hall liquid using a few-electron bubble. *Phys. Rev. B*, 66(125308):1+, September 2002.

[9] Saul A. Teukolsky William H. Press, Brian P. Flannery and William T. Vetterling. *Numerical Recipes in C : The Art of Scientific Computing.* Cambridge University Press, 1992.

[10] James W. Demmel. *Applied Numerical Linear Algebra.* Soc. for Industrial and Applied Math, 1997.